ACS Infectious Diseases

Article

Targeting Mobilization of Ferrous Iron in Pseudomonas aeruginosa Infection with an Iron(II)-Caged LpxC Inhibitor

Brian Blank, Poulami Talukder, Ryan Muir, Erin Green, Eric P Skaar, and Adam R. Renslo

ACS Infect. Dis., **Just Accepted Manuscript** • DOI: 10.1021/acsinfecdis.9b00057 • Publication Date (Web): 29 May 2019

Just Accepted

is published by the American Chemical Society. 1155 Sixteenth Street N.W., Washington, DC 20036

Targeting Mobilization of Ferrous Iron in *Pseudomonas aeruginosa* Infection with an Iron(II)-Caged LpxC Inhibitor

Brian R. Blank,[†,‡] Poulami Talukder,[†,‡] Ryan K. Muir,[†] Erin R. Green,[§] Eric P. Skaar,[§] and Adam R. Renslo[†,*]

†Department of Pharmaceutical Chemistry, University of California, San Francisco, 600 16th Street, San Francisco, CA 94158.

§Department of Pathology, Microbiology, and Immunology, Vanderbilt University Medical Center, 1161 21st Avenue South, Medical Center North, Nashville, TN 37232

E-mail: adam.renslo@ucsf.edu

Iron is essential to all life and competition for this vital nutrient is central to host-pathogen interaction during infection. The opportunistic Gram-negative pathogen *Pseudomonas aeruginosa* utilizes a diverse array of iron acquisition strategies, including those enabling import of extracellular ferrous iron. We hypothesize that soluble and redox-active ferrous iron can be employed to activate caged antibiotics at site(s) of infection *in vivo*. Here we describe new chemistry that expands the application of our laboratory's Fe^{2+}-activated prodrug chemistry to cage hydroxamic acids, a class of drugs that present manifold development challenges. We synthesize the caged form of a known LpxC inhibitor and show that it is efficacious in an acute *P. aeruginosa* mouse lung infection model, despite showing little activity in cell culture experiments. Overall, our results are consistent with the Fe^{2+}-promoted uncaging of an antibacterial payload at sites of infection in an animal, and lend support to recent reports indicating that extracellular pools of ferrous iron can be utilized by bacterial pathogens like *P. aeruginosa* during infection.

Keywords: host-pathogen interaction, iron acquisition, nutrient acquisition, targeted prodrugs, caged antibiotics, tissue targeting

Iron is the fourth most abundant element in the earth's crust and may have played a key role in the emergence of life in the reducing atmosphere of the pre-biotic earth[1]. The ubiquity of iron-mediated chemistry in contemporary biology is thus unsurprising. Iron cofactors redox cycle between the ferrous (Fe^{2+}) and ferric (Fe^{3+}) states, performing a wide array of useful redox chemistry and thereby enabling cellular processes. Under aerobic conditions at physiological pH, iron exists in the insoluble ferric state, and so the transport and storage of iron in biology requires various chaperones (e.g. transferrin, lactoferrin, ferritin, siderophores, etc.) that bind, solubilize, and render redox-inert the Fe^{3+} ion. The much more soluble Fe^{2+} ion redox cycles, promoting Fenton chemistry that is toxic to cells.[2]

Competition between bacterial populations for iron resources has seen remarkable adaptions in iron acquisition strategies and pathways. The Gram-negative bacterium *Pseudomonas aeruginosa*, for example, is able to express transporters for the iron siderophores of competing bacterial species in addition to those for its cognate siderophores pyoveridine and pyochelin.[3] The pathogen also utilizes non-siderophore based iron uptake via dedicated transporters of heme(II)iron and inorganic Fe^{2+} present in the extracellular milieu, or pried from host heme/iron proteins[4] (Figure 1). Iron acquisition and withholding similarly lies at the heart of host-pathogen interactions,[4-7] nutritional immunity,[8-9] and the mammalian response to bacterial infection. This response includes the production of lactoferrin to sequester Fe^{3+} and the release of hepcidin, a negative regulator or iron export, which leads to host withholding of iron (as Fe^{3+}) in macrophages and the liver.

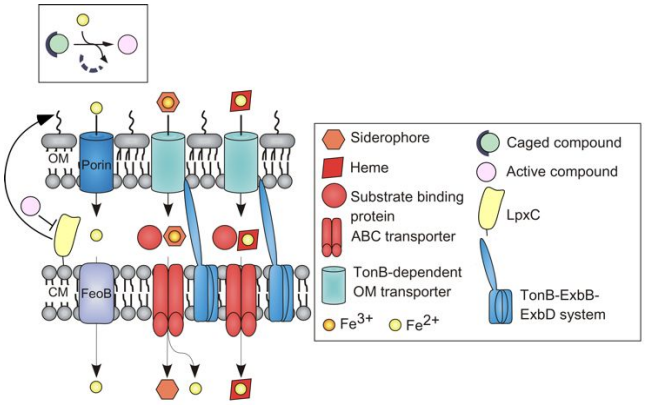

Figure 1. Diverse iron uptake strategies of *P. aeruginosa* are united by the mobilization of ferrous iron (yellow spheres) in various cellular and extracellular compartments. In the approach described herein, an antibacterial prodrug (in box, green) is uncaged and activated by ferrous iron.

In a recent report, Nolan and co-workers[10] showed that sequestration of the reduced Fe^{2+} ion by the human calprotectin protein induces an iron starvation response in *P. aeruginosa.* This finding implies that the Fe^{2+} ion is a bioavailable source of iron during infection by certain bacterial pathogens. Notably, antibacterial strategies that specifically target pools of the reduced Fe^{2+} ion have been

essentially unknown to date. Instead, prior efforts have focused on the ferric ion (Fe^{3+}) and the various siderophores that are required to solubilize and transport iron in this oxidation state. Thus, a wide array of siderophore-antibiotic conjugates or 'sideromycins' have been described, many with impressive activity and an expanded antimicrobial spectrum.[11-15] This approach is not without challenges however. Preclinical investigations of the siderophore-monobactam agents MB-1 and SMC-3176, for example, have revealed an adaptive resistance mechanism in which certain *P. aeruginosa* strains overexpress pyoveridine siderophore as a means to prevent sideromycin uptake.[16-17] As well, selection of SMC-3176-resistant strains identified various resistance mutations to bacterial iron uptake genes. Nevertheless, the siderophore-cephalosporin cefiderocol (S-649266)[18] is currently progressing through human clinical trials and is apparently less impacted by these resistance mechanisms than the earlier siderophore-monobactams.

Whereas exploiting uptake of Fe^{3+} suggests a siderophore-based approach, we reasoned that targeting pools of Fe^{2+} could instead leverage a reactivity-based approachinvolving Fenton-type chemistry of organic peroxides. In fact, safe and well-tolerated antimalarials including the artemisinins and synthetic 1,2,4-trioxolanes arterolane[19] and artefenomel[20] provide clinical precedent for iron(II)-dependent pharmacology based on Fenton chemistry. In recent years, our lab has described arterolane-inspired scaffolds[21-22] (denoted TRX) that re-imagine the 1,2,4-trioxolane ring as a caging moiety and molecular sensor of the Fe^{2+} ion, and that incorporate a traceless linker to drug payloads (Figure 2).

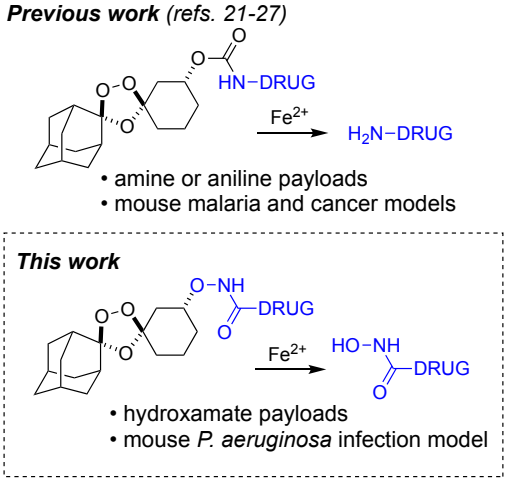

Figure 2. Representative structure of iron(II)-sensing trioxolane prodrugs described by our group previously (top) and the new caged hydroxamates described herein.

Previous *in vivo* studies of TRX conjugates have demonstrated enhanced efficacy and tolerability in malaria infection models for iron(II)-caged forms of a preclinical parasite cysteine protease inhibitor[23] and the antimalarial mefloquine.[24] Similarly, TRX-caged forms of a duocarmycin-class chemotherapeutic showed enhanced tolerability and efficacy in xenograft models.[25] The same chemistry has likewise been applied to produce TRX-PURO[26] and ICL-1,[27] new cellular and *in vivo* probes of Fe^{2+} that exhibit remarkable metal ion and oxidation-state specificity, and that are stable toward other cellular reductants such as glutathione and cysteine.

In the context of a bacterial infection, TRX-antibiotic conjugates were envisioned to exploit extracellular pools of Fe^{2+} and possibly also periplasmic and cytoplasmic Fe^{2+} liberated during the unloading of iron from siderophores (Figure 1). The *in vitro* and *in vivo* activities of such antibiotic conjugates might also provide insights into reduced forms of iron in the microenvironment of infection. Indeed, a recent study[27] of the TRX-based probe ICL-1 revealed a mobilization of Fe^{2+} in mice infected with the Gm-negative pathogen *A. baumannii*.

Many existing antibiotics possess the requisite amine functionality required for conjugation the TRX moiety. However, to expand the scope of this approach, we describe here new chemistry that enables conjugation of hydroxamate drug payloads (Figure 2). We use this chemistry to prepare the iron(II)-caged form of a known LpxC inhibitor and study its antimicrobial effects across a large panel of Gm-negative pathogens and in a *P. aeruginosa* mouse acute lung infection model. Notably, we find the iron(II)-caged agent to be efficacious *in vivo*, despite having little activity in the context of an *in vitro* MIC experiment. Taken together, our findings support the idea that ferrous iron is a bioavailable iron source during infection, and suggest this redox-active species can be exploited to activate iron(II)-caged antibiotics at site(s) of infection.

RESULTS and DISCUSSION

The emergence of carbapenem-resistant *Enterobacteriaceae* (CRE) and multidrug resistant *P. aeruginosa* highlights the need for new drug targets and technologies to address these pathogens.[28-30] Among several promising drug targets being explored is UDP-3-O-(*R*-3-hydroxymyristoyl)-*N*-acetylglucosamine deacetylase (LpxC, a metallo-deacetylase that performs the first committed step in Lipid A biosynthesis. Lipid A in turn serves as the membrane-anchoring component of lipopolysaccharide (LPS), an essential component of the outer membrane of Gm-negative bacteria.[31] Several *in vivo*-active hydroxamate-based LpxC inhibitors (LpxCi) have been described in the past decade,[32] including PF-5081090[33] and ACHN-975, which entered human clinical safety evaluation (Figure 3).[32] Frequencies of resistance to LpxC inhibitors are generally very low, with a value of $<5.0 \times 10^{-10}$ reported for PF-5081090 against *P. aeruginosa*.[33] However, the clinical challenges of advancing hydroxamate-based agents, including matrix metalloproteinase[34] and histone deacetylases[35] inhibitors, are well documented. These include inhibition of off-target metalloenzymes, metabolic and proteolytic instability of the hydroxamate function, and mutagenic

potential that likely results from Lossen rearrangement of *O*-activated hydroxamates to form DNA-reactive isocyanates.[35]

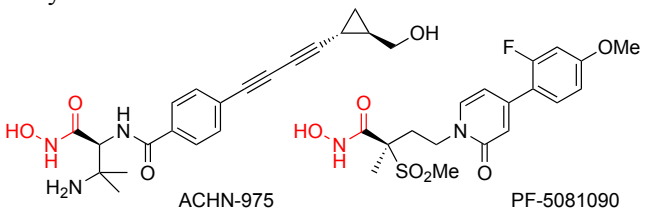

ACHN-975 PF-5081090

Figure 3. Clinical and pre-clinical stage LpxC inhibitors ACHN-975 and PF-5081090, respectively, based on hydroxamate metal-binding moieties (shown in red).

Caging a hydroxamate drug at the oxygen atom of the hydroxamate with the TRX moiety offers a possible means to address these liabilities. Blocking this crucial site would serve several purposes, namely 1) temporarily blocking on-target activity prior to activation by Fe^{2+}, 2) sterically occluding interaction with host metalloenzyme off-targets while in the caged form, and 3) preventing or mitigating Lossen rearrangement, which proceeds via oxygen atom activation (e.g., acylation). Here we aimed to prepare a TRX conjugate of the known LpxC inhibitor PF-5081090. A retro-synthetic analysis of putative TRX-LpxCi conjugates suggested a convergent disconnection at C–N of the hydroxamate (Figure 4). Following this disconnection required access to the LpxCi as a carboxylate and an aminooxy-substituted TRX intermediate. The former is typically the penultimate intermediate in the synthesis of hydroxamate-based agents, while the latter could, in principle, be prepared by Griesbaum co-ozonolysis reaction of a phthalimide protected 3-(aminooxy)cyclohexan-1-one (Figure 4).

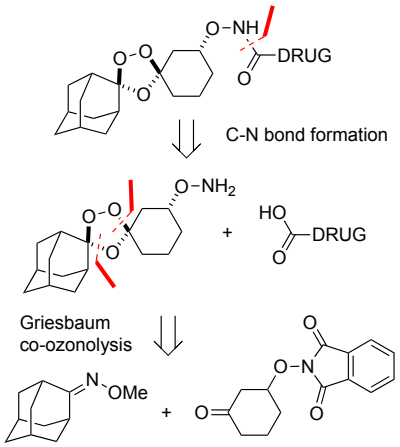

Figure 4. Retrosynthetic analysis of trioxolane-hydroxamate conjugates in which the hydroxamate oxygen atom serves as the site of conjugation to the TRX moiety.

After considerable experimentation, an efficient synthetic approach amenable to multi-gram scales was identified (Scheme 1). Thus, mono-benzylation of cyclohexane-1,3-diol afforded the desired ether **1**, which was subjected to Mitsunobu reaction with *N*-hydroxyphthalimide to afford **2**. Selective removal of the benzyl protecting group with BCl_3•SMe_2 proceeded in 89% yield to afford alcohol **3**. Unsurprisingly, oxidation of **3** to afford **4** was complicated by the propensity of **4** to undergo beta-elimination. Ultimately, we found that this conversion could be accomplished in good to high yields with the Dess-Martin reagent, or alternatively by Swern oxidation under carefully controlled conditions as detailed in the experimental section. Griesbaum co-ozonolysis reaction of **4** with adamantan-2-one *O*-methyl oxime afforded 1,2,4-trioxolane **5** in 92% yield based on **4**. We have reported[36] that this process generally proceeds with high diastereoselectivity favoring the *trans* isomer, and in the present case furnished **5** in an excellent 13:1 diastereomeric ratio (d.r.). Deprotection of **5** with hydrazine proceeded smoothly to afford the desired aminooxy TRX intermediate (±)-**6**. To further enable study of TRX conjugates derived from (±)-**6**, we also developed a route to the corresponding aminomethyl intermediate (±)-**7** (see Supporting Information). This material can be employed to prepare peroxidic control conjugates in which the drug payload is inactivated (i.e., amide rather than hydroxamate form).

Next, intermediates (±)-**6** and (±)-**7** were coupled to the known[37] carboxylic acid (±)-**8** (Scheme 2). This provided the final drug conjugate **9** and the amide-linked control **10** as diastereomeric mixtures that were evaluated as such in all subsequent bioassays (Scheme 2). We confirmed that **9** reacts cleanly with ferrous ammonium sulfate in PBS pH 7.4 and DMSO to liberate the ketone intermediate **9*** and then (±)-**11** as desired (Scheme 2 and Supporting Information). Control **10** possesses the same peroxide bond as **9** but cannot liberate an active hydroxamate, thus controlling for any peroxide-based contribution to the antimicrobial activity of **9**. In fact, **10** exhibited no measurable MIC in any of the strains tested, confirming that the TRX moiety in **9** serves as iron(II)-sensor and caging group, without significant antibacterial action of its own.

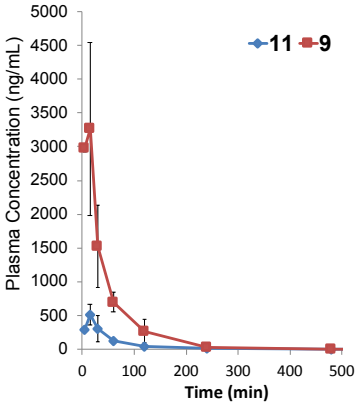

Figure 5. Plasma exposure profile of prodrug **9** (red) and systemically released **11** (blue) following a single IP dose of **9** (16 mg/kg) to healthy female NSG mice (n = 9).

To evaluate its *in vivo* stability and pharmacokinetic profile, **9** was administered by IP injection to female NSG mice and the resulting plasma samples analyzed for both

intact **9** and free LpxCi payload **11** that may have been released from **9** systemically by Fe^{2+} dependent or independent processes. Compound **9** exhibited a relatively rapid elimination profile ($T_{1/2}$ ~ 0.7 hr) similar to that reported for PF-5081090[37] (Figure 5). We also observed some systemic release of payload **11** from **9**, amounting to ca. 19% of the dose by AUC, or roughly 2-3 times the extent of release observed for TRX conjugates based on carbamate linker chemistry[25]. Although such systemic activation is undesirable, compound **9** nevertheless remained ~80% intact in the experiment, and exhibited sufficient *in vivo* exposure for evaluation in animal infection models.

First however, we performed *in vitro* microbiological evaluation of compounds **9**, **10** and **11** across a panel of Gram-negative pathogens and control strains. These included strains expressing common resistance factors (mainly β-lactamases) and variable efflux pump expression phenotypes (Table 1). MICs were determined according to CLSI standards[38-39] in both in cation adjusted Mueller Hinton II broth (CAMHB) and also in ID-CAMHB media that had been depleted of iron by treatment with Chelex. Iron-depleted media is typically used to study siderophore-antibiotic conjugates in MIC experiments, as these conditions are expected to activate the bacterial iron uptake pathways that are exploited by such agents. Here, we employed iron-depleted media both to evaluate the possible effect of activating Fe^{3+} uptake pathways on prodrug activation, and also to control for spurious extracellular activation of **9** by iron in normal media.

Scheme 1. Stereocontrolled synthesis of key trioxolane intermediate **6** bearing a 3'-aminooxy function.

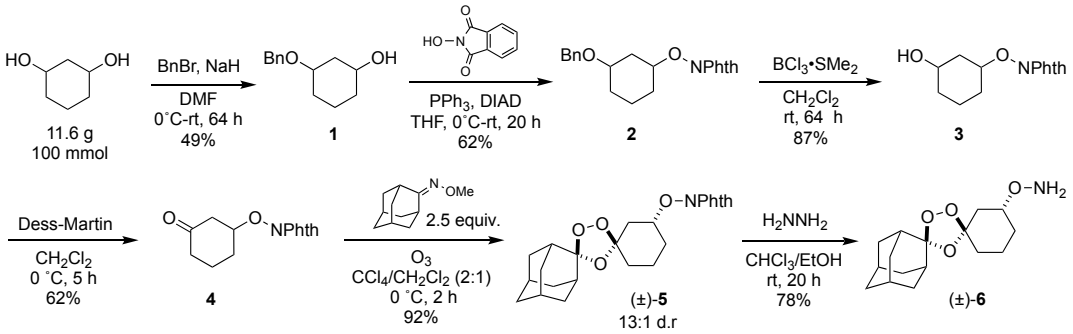

Scheme 2 Synthesis of hydroxamate- and amide-linked TRX conjugates **9** and **10** from known LpxC inhibitor **8** (top left). Compound **10** is chemically unable to release an LpxCi and serves as a control for any peroxide-derived antibacterial activity in **9**. Reaction of **9** with ferrous ammonium sulfate in PBS/DMSO (1:1) cleanly produces the intermediate **9*** and then free **11** as revealed by LC/MS (scheme below left and UV absorbance spectra at right).

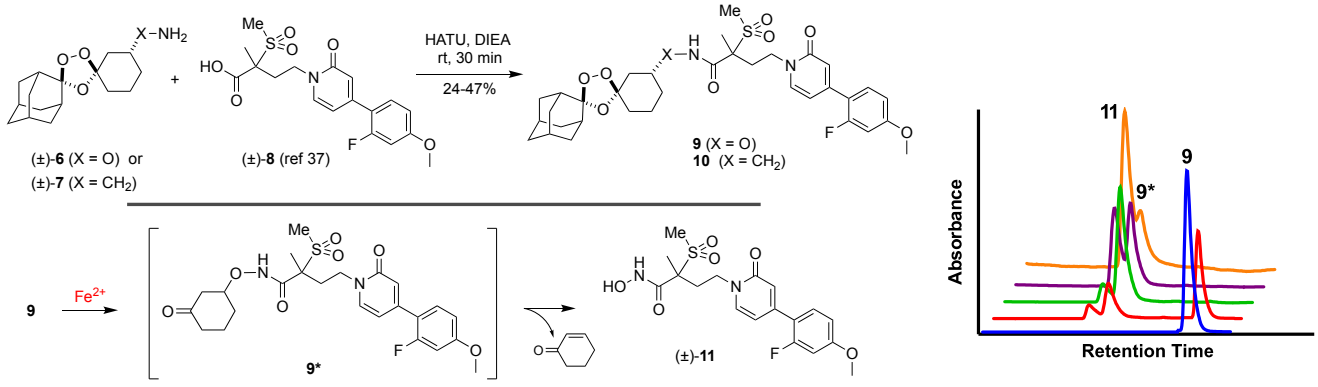

Accordingly, compounds **9-11** and antibiotic controls were tested under both conditions against twenty strains representing five different pathogens. We observed no measurable MIC for control **10** under any of the conditions (MICs > 64 mg/mL), indicating that the TRX moiety present in **10** and **9** lacks antimicrobial activity of its own (Table 1). The MICs obtained for **9** can therefore be inferred to derive primarily or solely from uncaging of the active LpxC inhibitor **11**. Differences in the MICs of **9** and **11** are thus interpreted as arising primarily from a combination of two factors, 1) the relative permeability of the compounds and access of **9** to intracellular Fe^{2+}, and 2) the efficiency of iron(II)-promoted uncaging of **9** assuming it can access intracellular Fe^{2+}. In fact, we observed the MICs of **9** to be ~8-fold higher than for **11** in *Escherichia coli* strains and ~16-fold higher in *Klebsiella pneumoniae*, *Enterobacter cloacae*, and *P. aeruginosa* strains. Both compounds were subject to efflux based on comparison of MICs for pump knockout and parental strains (Table 1). The MIC data thus suggest that **9** has limited access to intracellular Fe^{2+} in an MIC experiment, presumably due to poor membrane permeability and/or drug efflux.

We found that the MICs for both **9** and **11** were essentially unchanged whether performed in standard CAMHB media or in ID-CAMHB media (see Supporting Information for full data set). The lone exception was a single *E. coli* strain (MMX 119) in which the MICs of **9** and **11** were 16-fold and 4-fold higher, respectively, in ID-CAMHB media. Since this MIC shift was observed for both iron(II)-sensitive (**9**) and insensitive (**11**) compounds, the shift in the MMX 119 strain appears to be unrelated to iron uptake or mobilization. The lack of MIC shift for **9** in ID media also implies that the compound is stable in the standard media and does not undergo iron(II)-promoted activation outside the cell in MIC experiments. This is consistent with the good stability of TRX conjugates in mammalian cell culture media[26] and the expectation that extracellular iron in an aerobic MIC experiment will exist in the TRX-inert ferric state. We next sought to test the efficacy of **9** in an *in vivo* infection model where host-pathogen competition for iron resources was predicted to mobilize Fe^{2+} in infected tissues.[27]

Infection of the cystic fibrosis (CF) lung by bacterial pathogens, including *P. aeruginosa,* is associated with dramatic changes to iron homeostasis.[40] Ferrous iron levels in the sputum of CF patients can be correlated with severity of disease, and reach aberrant (mid-μM) concentrations in advanced disease,[41] likely due to an acidic and hypoxic microenvironment in the infected lung. The likely role of extracellular Fe^{2+} in *P. aeruginosa* infection is further supported by the existence in the pathogen of transporters for the Fe^{2+} ion (FeoA/B system) and by utilization of the host protein calprotectin to sequester the Fe^{2+} ion in response to infection.[10] Accordingly, the CF lung appears to possess a substantial reservoir of extracellular ferrous iron that promotes bacterial colonization and virulence, but might also be exploited for the tissue-selective delivery of antibiotics. Since a tractable and robust mouse model of CF is unavailable, we compared the efficacy of conjugate **9** to its parent LpxCi payload (**11**) in an acute lung infection model using the PA14 strain of *P. aeruginosa*.[42]

Table 1. MICs of compounds 9-11 and antibiotic controls against diverse Gm-negative pathogens in CAMBH media.[a]

Test Organisms	MMX./ATCC No.	Phenotype	MIC (μg/mL) of Test Compounds and Controls				
			11	**10**	**9**	**Imipenem**	**Ceftazidime/ Avibactam**
E. coli	5684/13352	TEM-10	1	>64	8	0.25	0.5/4
	6839/BAA-2326	CTX-M-15	0.5	>64	4	0.12	0.12/4
	5980	NDM-1	0.25	>64	2	8	>64/4
	119	Parent (TolC Knockout)	0.25	>64	2	0.12	0.12/4
	121	TolC Knockout	≤0.06	>64	0.12	0.25	0.12/4
	102/25922	QC	0.5	>64	16	0.12 (0.06-0.25)	1/4 (1/4-4/4)
K. pneumoniae	537/700603	SHV-1	4	>64	>64	0.25	1/4
	4683	KPC-2	4	>64	>64	8	0.5/4
	4692	KPC-3	2	>64	>64	>64	2/4
	5979	NDM-1	8	>64	>64	64	>64/4
E. cloacae	6308	MEM-R	4	>64	64	16	4/4
	7941	AmpC	0.5	>64	16	0.25	1/4
	5981	NDM-1	8	>64	>64	>64	>64/4
P. aeruginosa	3476	Parent (mexAB/oprM KO)	1	>64	16	1	2/4
	3477	mexAB/oprM Knockout	≤0.06	>64	0.5	1	0.5/4
	4698	VIM-2	2	>64	64	>64	32/4
	4654	IMP-7	2	>64	>64	>64	>64/4
	PA14		1.5	–	30	–	–
	103/27853	QC	2	>64	>64	1 (1-4)	2/4 (0.5/4-4/4)
A. baumannii	1630/19606	Wild type	>64	>64	>64	0.25	64/4
	4651	OXA-27	>64	>64	>64	64	64/4

[a]CLSI QC ranges shown below MIC where applicable; see Supporting Information for MICs in CAMHB-ID media. All MIC determinations (except PA14) were performed at Micromyx, LLC (Kalamazoo, MI).

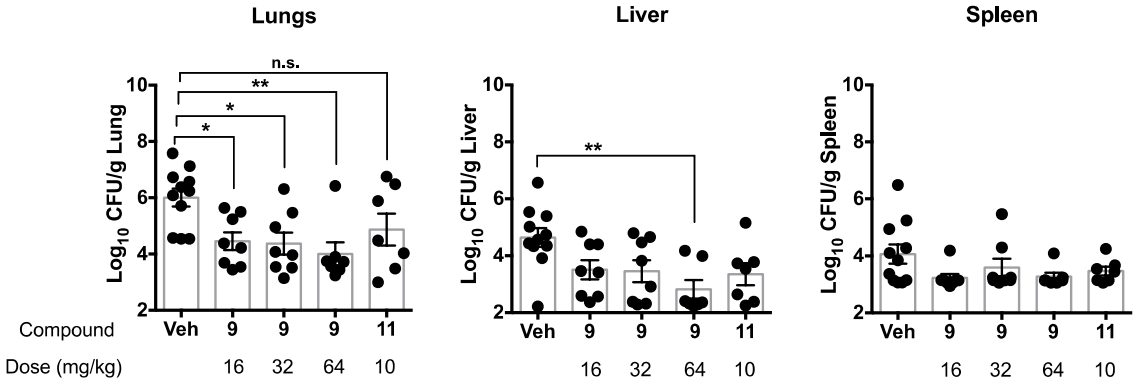

Figure 6. Bacterial colony forming units (CFU) in lung, heart and spleen in mice infected with PA14 strain *P. aeruginosa* 24 hours after being treated with dosing vehicle (Veh), a single IP dose of **11** (10 mg/kg), an equimolar IP dose of **9** (16 mg/kg), or two- or four-fold higher doses of **9**. * $p < 0.05$, ** $p < 0.01$. Error bars represent standard error of the mean.

First, we confirmed that the LpxCi payload **11** delivered from **9** was active against PA14 *P. aeruginosa*. Indeed, compound **11** exhibited activity (PA14 MIC = 1.5 μg/mL) at concentrations that seemed likely to be achieved *in vivo*, assuming effective uncaging of **9 (**to liberate **11**) at the infection site. The MIC of **9** against this strain was weaker, as expected (MIC = 30 μg/mL), and consistent with the MIC shifts observed across the larger panel of isolates (Table 1).

Next, wildtype female BALB/c mice were inoculated intranasally with $1x10^5$ CFU/mL of PA14 strain *P. aeruginosa* as described previously.[42] At two and six hours post-inoculation, mice were injected intraperitoneally with vehicle, active LpxCi **11** (10 mg/kg), or the iron(II)-caged LpxCi **9** at an equimolar dose (16 mg/kg), or at a two-fold (32 mg/kg), or four-fold (64 mg/kg) higher dose. Bacterial colony forming units (CFU) were assessed at 24 hrs post-inoculation in lung, liver, and spleen (Figure 6). Bacterial load was highest in the lung and so this tissue provided the data most useful for comparison of treatment arms. Surprisingly, administration of **11** directly had only a modest effect on bacterial load that was not statistically different from vehicle treated controls. By contrast, and despite its much weaker MICs, the iron(II)-caged form **9** significantly reduced bacterial load over vehicle control at both the equimolar dose (16 mg/kg) and at the two higher dosing levels. Compound **9** was well tolerated even at the highest, 64 mg/kg dose. Bacterial CFU counts were significantly lower in liver, below the limit of detection in some animals. Nevertheless, compound **9** at the 64 mg/kg dose exhibited a significant reduction in CFU over vehicle controls in liver. Bacterial loads in spleen were below the limit of detection in the majority of the animals and thus provided no interpretable data.

The superior efficacy of **9** compared to **11** in this model is consistent with the selective uncaging of **9** at sites of infection, most likely by extracellular Fe^{2+} in the microenvironment. This inference is based on the observation that intact **9** exhibited little antimicrobial effect in the MIC experiment where only intracellular or periplasmic Fe^{2+} is available for activation. The possible role of the endoperoxide function in the superior *in vivo* efficacy of **9** is ruled out by the complete lack of activity observed for control compound **10**. Although we cannot strictly rule out the contributions of alternate mechanisms of *in vivo* activation, extensive characterization of diverse TRX conjugates by our laboratory[26] and others[27] suggests that, among biologically relevant reducing agents, Fe^{2+} is by far the most likely to be involved in their activation, and particularly in the mode of activation that leads to release of free drug payload.

Notably, access of **9** to intracellular Fe^{2+} in the MIC experiment was quite limited, leading to inferior MICs compared to **11** (Table 1). This suggests that host-pathogen interaction in the live animal mobilizes Fe^{2+} in infected tissues to an extent that is not mimicked in MIC experiments. In part this difference may derive from liberation of reduced iron from host proteins (carriers and enzymes) during active infection, producing reservoirs of extracellular Fe^{2+} that can uncage TRX prodrugs and concentrate antibiotic payload in the infection microenvironment. This proposed mechanism of action for **9** would be consistent with the *in vivo* behavior of ICL-1[27], wherein Fe^{2+}-mediated release of aminoluciferin payload was correlated with *A. baumanii* infection in several tissues.

Here we have presented a prototypical iron(II)-caged LpxC inhibitor and *in vivo* data suggesting its activation at sites of infection in an animal. The use of such agents could enable concentration of antibiotic at sites of

infection while mitigating inhibition of metalloenzyme off-targets, though the latter feature remains to be tested explicitly. The *in vivo* results presented here are consistent with emerging evidence[10, 27, 41] that competition for Fe^{2+}, like that for Fe^{3+}, is an important aspect of host-pathogen interaction during infection. We propose here that this reactive iron pool can be exploited for tissue-selective uncaging of antibacterial agents *in vivo*, and that this approach may enhance efficacy and tolerability. Further studies, including optimization of the TRX moiety for antibacterial applications and use of this new approach to deliver other antibacterial payloads are ongoing in our laboratories and will be reported in due course.

METHODS

Synthesis. Intermediate **8** was prepared as described.[37] General synthetic methods and specific procedures for the synthesis of intermediate **7** and control **10** are provided as Supporting Information.

3-(benzyloxy)cyclohexan-1-ol (1). To a round bottom flask equipped with an argon inlet adapter, stirbar, and rubber septum was charged with a solution of 1,3-cyclohexanediol (11.62 g, 100 mmol, 1.0 equiv.) in DMF (170 mL). The solution was cooled at 0 ˚C to which was slowly added sodium hydride (60% dispersion in mineral oil, 4.2 g, 105 mmol, 1.05 equiv). The suspension was allowed to warm to room temperature and stirred for 1 hour, and then cooled to 0 ˚C. Benzyl bromide (12.74 mL, 105 mmol, 1.05 equiv) was then added and the reaction mixture stirred at 0 ˚C for 50 minutes, after which the cooling bath was removed and the mixture stirred for 63 hours at ambient temperature. The reaction mixture was then diluted with 150 mL of satd. aq. NaCl, 200 mL of 10% HCl and 100 mL of EtOAc. The aqueous layer was separated and extracted with two 100 mL portions of EtOAc. Solid NaCl was then added to the aqueous layer and further extracted with four 100 mL portions of EtOAc. The combined organic layers were washed with 100 mL of satd. aq. NaCl, dried over Na_2SO_4, filtered, and concentrated under reduced pressure to afford a yellow oil. The crude product was purified by column chromatography (0–50% EtOAc/hexanes gradient elution) to yield **1** (10.133 g, 49%) as a yellow oil. Based on ^{1}H NMR analysis, the product exists as a 6:1 mixture of diastereomers. ^{1}H NMR (400 MHz, $CDCl_3$) δ 7.35–7.27 (m, 4H), 7.27–7.22 (m, 1H), 4.58–4.46 (m, 2H), 4.09–4.00 (m, 1H, minor diastereomer), 3.81–3.74 (m, 1H, minor diastereomer), 3.73–3.64 (m, 1H), 3.55–3.45 (m, 1H), 2.14–2.04 (m, 1H), 1.88–1.68 (m, 3H), 1.68–1.54 (m, 1H), 1.53–1.33 (m, 2H), 1.31–1.18 (m, 1H); ^{13}C NMR (100 MHz, $CDCl_3$) δ 138.9 (minor diastereomer), 138.5, 128.3, 128.2 (minor diastereomer), 127.4, 127.4 (minor diastereomer), 127.3, 127.2 (minor diastereomer), 75.3, 73.9 (minor diastereomer), 70.1, 69.8 (minor diastereomer), 68.2, 66.8 (minor diastereomer), 39.4, 39.1 (minor diastereomer), 34.1 (minor diastereomer), 34.1, 30.3, 30.1 (minor diastereomer), 19.0, 18.3 (minor diastereomer); MS (ESI) calculated for $C_{13}H_{19}O_2$ $[M + H]^+$ *m/z* 207.14, found 206.92.

3-(benzyloxy)cyclohexyl phthalimidyl ether (2). A round bottom flask equipped with an argon inlet adapter, stirbar, and rubber septum was charged with a solution of alcohol **1** (6.188 g, 30 mmol, 1.0 equiv) in THF (300 mL). To the solution was added N-hydroxyphthalimide (5.550 g, 33 mmol, 1.10 equiv) and triphenylphosphine (8.743 g, 33 mmol, 1.10 equiv). After cooling the solution to 0˚C, diisopropyl azodicarboxylate (6.86 mL, 34.5 mmol, 1.15 equiv) was added dropwise and the mixture maintained at 0˚C for 90 min, after which it was allowed to warm to room temperature and stirred for 19 hours. The reaction mixture was then concentrated under reduced pressure and diluted with 200 mL of EtOAc and 100 mL of satd. aq. $NaHCO_3$. The layers were separated and the organic phase was washed with four 100 mL portions of satd. aq. $NaHCO_3$. The aqueous layer was then extracted with a 100 mL portion of EtOAc and the combined organic layers washed with 100 mL satd. aq. NaCl, dried over Na_2SO_4, filtered, and concentrated to yield a yellow oil. The crude residue was purified by flash column chromatography (0–30% EtOAc/Hexanes gradient elution) to afford **2** (6.618 g, 62%) as a clear colorless oil that solidified upon standing at 4˚C. ^{1}H NMR (400 MHz, $CDCl_3$) δ 7.85–7.78 (m, 2H), 7.76–7.70 (m, 2H), 7.36–7.17 (m, 5H), 4.61–4.44 (m, 3H), 4.02–3.88 (m, 1H), 2.08–1.94 (m, 2H), 1.90–1.56 (m, 6H); ^{13}C NMR (100 MHz, $CDCl_3$) δ 164.2, 138.9, 138.6 (minor diastereomer), 134.4 (minor diastereomer), 134.3, 128.9, 128.9 (minor diastereomer), 128.3 (minor diastereomer), 128.2, 127.5 (minor diastereomer), 127.5, 127.3, 123.5 (minor diastereomer), 123.4, 84.2 (minor diastereomer), 83.6, 75.5 (minor diastereomer), 73.7, 70.2, 70.1 (minor diastereomer), 37.1 (minor diastereomer), 35.3, 31.3 (minor diastereomer), 30.4 (minor diastereomer), 30.3, 29.7, 20.2 (minor diastereomer), 18.9; MS (ESI) calculated for $C_{21}H_{22}NO_4$ $[M + H]^+$ *m/z* 352.15, found 352.07.

3-(phthalimidyloxy)cyclohexan-1-ol (3). A round bottom flask equipped with an argon inlet adapter, stirbar, and rubber septum was charged with a solution of benzyl ether **2** (2.108 g, 6 mmol, 1.0 equiv) in CH_2Cl_2 (100 mL). To the solution was added boron trichloride dimethyl sulfide solution (2.0 M in CH_2Cl_2, 32 mL, 64 mmol, 10.7 equiv) dropwise via syringe. The mixture was stirred at room temperature for 63 hours, at which point the reaction mixture was added in 10 mL portions to an Erlenmeyer flask containing a stirring mixture of CH_2Cl_2 (100 mL) and satd. aq. $NaHCO_3$ (100 mL). The organic phase was collected and washed with two 50 mL portions of satd. aq. $NaHCO_3$. The combined aqueous layers were extracted thrice with 100 mL portions of CH_2Cl_2 and the combined organic phases washed with 100 mL satd. aq. NaCl, dried over Na_2SO_4,

filtered, and concentrated under reduced pressure to afford a brown oil. The crude residue was purified by flash column chromatography (0–75% EtOAc/Hexanes gradient elution) to yield **3** (1.361 g, 87%) as a light orange solid. ^{1}H NMR (400 MHz, $CDCl_3$) δ 7.87–7.80 (m, 2H), 7.79–7.72 (m, 2H), 4.64–4.55 (m, 1H), 4.35–4.26 (m, 1H), 2.15–2.05 (m, 1H), 1.94–1.76 (m, 5H), 1.76–1.54 (m, 2H), 1.53–1.42 (m, 1H); ^{13}C NMR (100 MHz, $CDCl_3$) δ 164.2, 134.4, 128.9, 123.5, 83.5, 66.6, 37.9, 33.6, 29.4, 18.8; MS (ESI) calculated for $C_{14}H_{16}NO_4$ $[M + H]^+$ *m/z* 262.11, found 261.98.

3-(phthalimidyloxy)cyclohexan-1-one (4). A round bottom flask equipped with an argon inlet adapter, stirbar, and rubber septum was charged a solution of alcohol **3** (0.638 g, 2.4 mmol, 1.0 equiv.) in CH_2Cl_2 (25 mL). The solution was cooled at 0˚C and then Dess-Martin periodinane (1.363 g, 3.1 mmol, 1.2 equiv.) was added in one portion. The solution was allowed to come to room temperature and stirred for 5 hours. The reaction mixture was then treated with 50 mL of CH_2Cl_2 and 50 mL of satd. aq. $NaHCO_3$. The organic layer was collected and washed with two 50 mL portions of satd. aq. $NaHCO_3$, one 50 mL portion of satd. aq. NaCl, dried over anhydrous Na_2SO_4, filtered, and concentrated under reduced pressure to deliver a colorless oil. The crude residue was purified by column chromatography (0-40% EtOAc/hexanes) to afford the product **4** (0.390 g, 62%) as a colorless oil ^{1}H NMR (400 MHz, DMSO) δ 7.86 (s, 4H), 4.70–4.58 (m, 1H), 2.80 (dd, *J* = 14.9, 4.6 Hz, 1H), 2.62 (dd, *J* = 14.8, 6.8 Hz, 1 H), 2.38–2.25 (m, 2 H), 2.19–2.00 (m, 2H), 2.00–1.90 (m, 1H), 1.73–1.60 (m, 1H); ^{13}C NMR (100 MHz, DMSO) δ 207.5, 163.7, 134.7, 128.6, 123.2, 84.6, 45.5, 40.1, 27.7, 19.5; MS (ESI) calculated for $C_{14}H_{14}NO_4$ $[M + H]^+$ *m/z* 260.09, found 259.90.

Alternate Conditions (Swern): To a solution of DMSO (1.1 mL, 15.5 mmol, 3.07 equiv) in CH_2Cl_2 (25 mL), cooled to –78 ˚C, was added oxalyl chloride (0.641 mL, 7.58 mmol, 1.5 equiv) dropwise via syringe. This solution was allowed to stir at –78 ˚C for 30 minutes, after which a solution of alcohol **3** (1.32 g, 5.05 mmol, 1.0 equiv) pre-dissolved in CH_2Cl_2 (15 mL) was added dropwise to the mixture over a period of 5 minutes, rinsing the vessel with two additional 5 mL portions of CH_2Cl_2. Triethylamine (5 mL, 35.9 mmol, 7.1 equiv; use of excess important) was then added dropwise to the solution over 2 minutes, and the resulting mixture was allowed to stir at –78 ˚C for 90 min. At this time, saturated aqueous citric acid (40 mL) was added directly to the reaction mixture while at –78 ˚C (important). To the frozen mixture was added additional CH_2Cl_2 (40 mL) and 20 mL of saturated aqueous citric acid, after which the frozen mixture was allowed to warm to ~4 ˚C over ca. 20 minutes. Once the mixture had thawed, the layers were separated and the organic layer was washed with additional saturated aqueous citric acid (20 mL). The combined aqueous layers were then extracted thrice with 40 mL portions of CH_2Cl_2. The combined organic layers were then washed with saturated aqueous $NaHCO_3$ (50 mL x 3), and brine (50 mL), dried over anhydrous Na_2SO_4, filtered, and concentrated under reduced pressure to afford **4** (1.23 g, 94% crude yield) as a yellow-orange solid.

3''-phthalimidyloxydispiro[adamantane-2,3'-[1,2,4]trioxolane-5',1''-cyclohexane] (5). A round bottom flask equipped with a stirbar was charged with a solution of ketone **4** (0.438 g, 1.689 mmol, 1.0 equiv) in carbon tetrachloride (20 mL) and dichloromethane (10 mL). To this solution was added adamantan-2-one *O*-methyl oxime (0.606 g, 3.379 mmol, 2.0 equiv) and the solution cooled to 0 ˚C and sparged with O_2 for 10 minutes. The reaction mixture was maintained at 0˚C while ozone was bubbled (2 L/min, 40% power) through the solution. After stirring for 50 mins, additional oxime (0.151 g, 0.842 mmol, 0.5 equiv), carbon tetrachloride (10 mL) and dichloromethane (10 mL) were added in a single portion to the reaction. Ozone was bubbled through the reaction for another 50 mins, at which point the reaction was judged complete by LCMS and TLC analysis. The solution was sparged with O_2 for 10 minutes to remove dissolved ozone, and then sparged with argon gas for 10 minutes to remove any dissolved oxygen. The solution was concentrated under reduced pressure to provide a viscous oil. The crude residue was purified by flash column chromatography (0–20% EtOAc/hexanes gradient elution) to afford **5** (0.665 g, 92%) as a white foamy solid. NMR analysis suggested a 13:1 d.r. in favor of the *trans* diastereomer. ^{1}H NMR (400 MHz, $CDCl_3$) δ 7.87–7.80 (m, 2H), 7.79–7.72 (m, 2H), 4.49–4.40 (m, 1 H, minor diastereomer), 4.31–4.18 (m, 1H), 2.50–2.41 (m, 1H), 2.41–2.35 (m, 1H, minor diastereomer), 2.24–2.15 (m, 1H), 2.03–1.92 (m, 5H), 1.92–1.72 (m, 7H), 1.72–1.61 (m, 6H), 1.52–1.36 (m, 2H); ^{13}C NMR (100 MHz, $CDCl_3$) δ 164.1, 134.5, 128.9, 123.5, 111.7, 108.8, 83.9, 39.5, 36.7, 36.2, 36.2, 34.8, 34.7, 34.7, 33.6, 29.6, 26.8, 26.4, 19.6; MS (ESI) calculated for $C_{24}H_{27}NO_6Na$ $[M + Na]^+$ *m/z* 448.17, found 448.04.

***O*-(dispiro[adamantane-2,3'-[1,2,4]trioxolane-5',1''-cyclohexan]-3''-yl)hydroxylamine (6)**. A round bottom flask equipped with an argon inlet adapter, stirbar, and rubber septum was charged with a solution of trioxolane **5** (0.640 g, 1.504 mmol, 1.0 equiv) in chloroform (18 mL) and ethanol (7 mL). To the solution was added hydrazine monohydrate (0.285 mL, 3.761 mmol, 2.5 equiv) and the mixture allowed to stir at room temperature for 20 hours. At this point, the solution was filtered through a glass fritted funnel to remove precipitated material and the filter cake washed well with CH_2Cl_2. The resulting filtrate was dried over anhydrous Na_2SO_4, filtered, and concentrated under reduced pressure to afford a white solid. The crude residue was then purified by flash column chromatography (0–20% EtOAc/hexanes gradient elution) to yield **6** (0.346 g, 78%) as a slightly orange solid. ^{1}H NMR analysis revealed a 13:1 d.r. in favor of

the *trans* diastereomer. ^{1}H NMR (400 MHz, $CDCl_3$) δ 5.27 (br s, 2H), 3.85–3.76 (m, 1H, minor diastereomer), 3.70–3.56 (m, 1H), 2.35–2.24 (m, 1H), 2.20–2.13 (m, 1H, minor diastereomer), 2.08–1.86 (m, 8H), 1.86–1.63 (m, 10H), 1.63–1.50 (m, 1H), 1.49–1.35 (m, 1H), 1.21–1.07 (m, 1H); ^{13}C NMR (100 MHz, $CDCl_3$) δ 111.5 (minor diastereomer), 111.3, 109.2, 108.9 (minor diastereomer), 79.7, 79.5 (minor diastereomer), 39.3, 38.8 (minor diastereomer), 36.7, 36.3, 36.3, 34.9 (minor diastereomer), 34.8, 34.8, 34.7, 34.7, 34.1, 29.7, 29.4 (minor diastereomer), 26.8, 26.4, 19.8, 19.5 (minor diastereomer); MS (ESI) calculated for $C_{16}H_{26}NO_4$ $[M + H]^+$ *m/z* 296.19, found 295.96.

***N*-(((*trans*-dispiro[adamantane-2,3'-[1,2,4]trioxolane-5',1''-cyclohexan]-3''-yl)oxy)-4-(4-(2-fluoro-4-methoxyphenyl)-2-oxopyridin-1(2*H*)-yl)-2-methyl-2-(methylsulfonyl)butanamide (9)**. To a vial charged with a stirred solution of acid 8 (13.0 mg, 0.034 mmol, 1 equiv) in DMF (0.5 mL) was added HATU (22.0 mg, 0.057 mmol, 1.5 equiv) and *N*,*N*-diisopropylethylamine (10 μL, 0.057 mmol, 1.5 equiv) at room temperature. The orange solution was allowed to stir for 15 mins, at which point a solution of intermediate 6 (12.0 mg, 0.042 mmol, 1.1 equiv) dissolved in DMF (0.5 mL) was added. The reaction mixture was stirred for an additional 15 mins, at which point the reaction was judged complete by TLC and LCMS analysis. The reaction mixutre was then diluted with with brine (20 mL) and extracted with two 10 mL portions of EtOAc. The combined organic layers were then dried over anhydrous Na_2SO_4, filtered, and concentrated under reduced pressure to afford an orange oil. The crude residue was purified by flash column chromatography (25 g silica gel cartridge, 0–100% EtOAc/hexanes, gradient elution) to afford the product contaminated with starting material. Further purification by rpHPLC provided pure 9 (6.0 mg, 24%) as a white solid. ^{1}H NMR (400 MHz, $CDCl_3$) δ 12.24 - 12.32 (m, 1H), 7.33 - 7.46 (m, 2H), 6.79 - 6.85 (m, 2H), 6.71 - 6.77 (m, 1H), 6.58 (br d, J = 6.82 Hz, 1H), 4.21 - 4.30 (m, 1H), 4.10 (br d, J = 4.87 Hz, 2H), 3.87 (s, 3H), 3.22 (d, J = 3.90 Hz, 3H), 2.46 - 2.61 (m, 3H), 2.35 - 2.45 (m, 1H), 2.20 - 2.27 (m, 1H), 1.83 - 2.08 (m, 10H), 1.66 - 1.80 (m, 10H), 1.43 (br d, J = 6.82 Hz, 2H); ^{13}C NMR (100 MHz, $CDCl_3$) δ 165.2, 165.1, 163.3, 163.3, 162.3, 162.2, 162.1, 159.7, 148.8, 137.0, 130.5, 130.5, 118.7, 118.7, 117.4, 117.3, 111.7, 111.0, 111.0, 109.2, 109.0, 109.0, 102.7, 102.4, 81.8, 81.6, 76.8, 69.0, 55.9, 48.4, 39.4, 39.3, 38.6, 38.5, 36.9, 36.4, 36.4, 36.3, 35.0, 34.9, 34.8, 34.5, 29.7, 29.6, 28.7, 27.0, 27.0, 26.6, 21.6, 21.5, 19.91, 19.88; MS (ESI) calculated for $C_{34}H_{44}FN_2O_8S$ $[M + H]^+$ *m/z* 675.28, found 675.11.

Microbiology. MICs for the panel of strains presented in Table 1 were performed under contract by Micromyx LLC (Kalamazoo, MI). The test isolates consisted of Gram-negative pathogens from the Micromyx repository; relevant quality control organisms from the American Type Culture Collection (ATCC) were included as directed by CLSI. The MIC assay method followed the procedure described by CLSI and employed automated liquid handling to conduct serial dilutions and liquid transfers.

A standardized inoculum of each organism was prepared per CLSI methods. Colonies were picked from the primary plate and a suspension was prepared to equal a 0.5 McFarland turbidity standard. Suspensions were diluted 1:20 in CAMBH (or ID-CAMBH) medium and then transferred to compartments of sterile reservoirs divided by length. A liquid handler was used dispense 10 μL of standardized inoculum into each well of the appropriate daughter plate for a final concentration of approximately 5 x 10^5 CFU per well. The wells of the daughter plates ultimately contained 185 μL of media, 5 μL of drug solution, and 10 μL of inoculum. Plates were stacked 3 high, covered with a lid on the top plate, placed into plastic bags, and incubated at 35ºC for 18-20 hr. Plates were viewed from the bottom using a plate viewer. An un-inoculated solubility control plate was observed for evidence of drug precipitation. MICs were read where visible growth of the organism was inhibited.

MIC testing of *P. aeruginosa* PA14 were performed in the Skaar lab as follows. Overnight cultures were sub-cultured 1:50 into fresh LB broth and grown for 1 hour. Bacteria were diluted 1:100 into medium containing increasing concentrations of either **9** (25-50 μg/mL) or **11** (0.25-1.5 μg/mL). Growth assays were carried out in 96 well plates in a 100 μL volume, and growth was measured by optical density absorbance at 600nm at 30 minute intervals. The MIC was defined as the minimum concentration of compound that inhibited growth over a period of 18 hours.

Pharmacokinetics Studies. Female NSG mice (n = 9 in three groups) were treated with a single intraperitoneal injection of **9** formulated in 50:40:10 PEG 400/20% 2-hydroxypropylcylcodextrine in water/DMSO. Blood samples were collected 5 min, 15 min, 30 min, 1 h, 2 h, 4 h, 8 h, 12 h, and 24 h after dosing (3 mice were sampled at each time point, with each group of three sampled thrice over 24 hrs). Plasma samples were analyzed for concentrations of **9** and **11** using MS/MS analysis at Integrated Analytical Solutions, Inc. (Berkeley, CA). The resulting data were analyzed with WinNonlin software to calculate standard PK parameters.

Infection Model. Wildtype BALB/c mice were purchased from Jackson Laboratories. All animal experiments were approved by the Vanderbilt University Medical Center Institutional Animal Care and Use Committee. Animal studies were not blinded. The murine model of *P. aeruginosa* pneumonia was performed as previously described[42]. Briefly, overnight cultures of *P. aeruginosa* PA14 were sub-cultured 1:1000 into fresh LB broth and grown for 3.5 hours to mid-exponential phase. Cultures were washed twice

with PBS, and resuspended in PBS at a density of 2.5×10^6 CFU/mL. Five to six-week old female mice were anesthetized with 2,2,2-tribromoethanol diluted in PBS and were infected intranasally with 1×10^5 CFU in 40 µL PBS. At 2 and 6 hours post-infection compounds were administered by intraperitoneal injection in an 80 µL volume as follows: compound **9** was administered at three doses: 16 mg/kg to 8 mice, 32 mg/kg to 8 mice, and 64 mg/kg to 7 mice. Compound **11** was administered to 7 mice at a dose of 10 mg/kg (equivalent to the 16 mg/kg dose of **9**). A vehicle control was administered to 11 mice. Compounds were formulated in a mixture of 10% DMSO, 8% 2-hydroxypropyl-beta-cyclodextrin, and 50% PEG400. At 24 hours post-infection, mice were euthanized, and lungs, livers, and spleens were sterilely harvested, homogenized, and plated onto LB agar for bacterial enumeration.

ASSOCIATED CONTENT

Supporting Information. Detailed synthetic procedures and characterization for compounds **7** and **10**. Scans of NMR spectra and LC/MS spectra for **9-11**. Supplemental tables and figures.

The Supporting Information is available free of charge on the ACS Publications website.

AUTHOR INFORMATION

Corresponding Author

Phone: 415-514-9698; Fax: 415-514-4507;
E-mail: adam.renslo@ucsf.edu.

ORCID
Adam R. Renslo: 0000-0002-1240-2846

Author Contributions

‡These authors contributed equally. B.R.B., P.T., and A.R.R. conceived of experiments. B.R.B, P.T., and R.K.M. synthesized compounds. E.P.S and E.R.G. designed the mouse infection model, which E.R.G. carried out. A.R.R. and R.K.M. drafted the manuscript and all authors reviewed and edited the manuscript.

Notes

The authors declare the following competing financial interest(s): A.R.R. holds equity in Tatara Therapeutics, Inc. which seeks to develop iron sensing therapies for cancer and infectious disease.

ACKNOWLEDGMENT

A. R. Renslo acknowledges funding from the US National Institutes of Health, R01 Grant AI105106. R. K. Muir acknowledges funding from the NIH Research Training Grant in Chemistry and Chemical Biology, T32 GM064337. Work in the E.P. Skaar laboratory was supported by R01 AI101171-08 and E. R. Green was supported by 5T32HL094296.

REFERENCES

1. De Duve, C., *Vital dust : life as a cosmic imperative*. Basic Books: New York, 1995; p xix, 362 p.
2. Winterbourn, C. C., Toxicity of iron and hydrogen peroxide: the Fenton reaction. *Toxicol. Lett.* **1995,** *82*, 969-974 DOI 10.1016/0378-4274(95)03532-x.
3. Ratledge, C.; Dover, L. G., Iron metabolism in pathogenic bacteria. *Annu. Rev. Microbiol.* **2000,** *54*, 881-941 DOI 10.1146/annurev.micro.54.1.881.
4. Palmer, L. D.; Skaar, E. P., Transition Metals and Virulence in Bacteria. *Annu. Rev. Genet.* **2016,** *50*, 67-91 DOI 10.1146/annurev-genet-120215-035146.
5. Skaar, E. P., The Battle for Iron between Bacterial Pathogens and Their Vertebrate Hosts. *PLoS Path.* **2010,** *6* (8), e1000949 DOI 10.1371/journal.ppat.1000949.
6. Soares, M. P.; Weiss, G., The Iron age of host–microbe interactions. *EMBO reports* **2015,** *16* (11), 1482 DOI 10.15252/embr.201540558.
7. Schaible, U. E.; Kaufmann, S. H., Iron and microbial infection. *Nat. Rev. Microbiol.* **2004,** *2* (12), 946-953 DOI 10.1038/nrmicro1046.
8. Hood, M. I.; Skaar, E. P., Nutritional immunity: transition metals at the pathogen-host interface. *Nat. Rev. Microbiol.* **2012,** *10* (8), 525-537 DOI 10.1038/nrmicro2836.
9. Weinberg, E. D., Nutritional immunity. Host's attempt to withold iron from microbial invaders. *JAMA* **1975,** *231* (1), 39-41 DOI 10.1001/jama.231.1.39.
10. Zygiel, E. M.; Nelson, C. E.; Brewer, L. K.; Oglesby-Sherrouse, A. G.; Nolan, E. M., The human innate immune protein calprotectin induces iron starvation responses in Pseudomonas aeruginosa. *J. Biol. Chem.* **2019**, 294, 3549-3562 DOI 10.1074/jbc.ra118.006819.
11. Miller, M. J.; Zhu, H.; Xu, Y.; Wu, C.; Walz, A. J.; Vergne, A.; Roosenberg, J. M.; Moraski, G.; Minnick, A. A.; McKee-Dolence, J.; Hu, J.; Fennell, K.; Kurt Dolence, E.; Dong, L.; Franzblau, S.; Malouin, F.; Mollmann, U., Utilization of microbial iron assimilation processes for the development of new antibiotics and inspiration for the design of new anticancer agents. *BioMetals* **2009,** *22* (1), 61-75 DOI 10.1007/s10534-008-9185-0.
12. Ji, C.; Juarez-Hernandez, R. E.; Miller, M. J., Exploiting bacterial iron acquisition: siderophore conjugates. *Future Med. Chem.* **2012,** *4* (3), 297-313 DOI 10.4155/fmc.11.191.
13. Mislin, G. L.; Schalk, I. J., Siderophore-dependent iron uptake systems as gates for antibiotic Trojan horse strategies against Pseudomonas aeruginosa. *Metallomics* **2014,** *6* (3), 408-420 DOI 10.1039/c3mt00359k.
14. Ghosh, M.; Miller, P. A.; Mollmann, U.; Claypool, W. D.; Schroeder, V. A.; Wolter, W. R.; Suckow, M.; Yu, H.; Li, S.; Huang, W.; Zajicek, J.; Miller, M. J., Targeted Antibiotic Delivery: Selective Siderophore Conjugation with Daptomycin Confers Potent Activity against Multidrug Resistant Acinetobacter baumannii Both in Vitro and in Vivo. *J. Med. Chem.* **2017,** *60* (11), 4577-4583 DOI 10.1021/acs.jmedchem.7b00102.
15. Schalk, I. J.; Mislin, G. L. A., Bacterial Iron Uptake Pathways: Gates for the Import of Bactericide Compounds. *J. Med. Chem.* **2017,** *60* (11), 4573-4576 DOI 10.1021/acs.jmedchem.7b00554.
16. Tomaras, A. P.; Crandon, J. L.; McPherson, C. J.; Banevicius, M. A.; Finegan, S. M.; Irvine, R. L.; Brown, M. F.; O'Donnell, J. P.; Nicolau, D. P., Adaptation-based resistance to siderophore-conjugated antibacterial agents by Pseudomonas aeruginosa. *Antimicrob. Agents Chemother.* **2013,** *57* (9), 4197-4207 DOI 10.1128/aac.00629-13.
17. Kim, A.; Kutschke, A.; Ehmann, D. E.; Patey, S. A.; Crandon, J. L.; Gorseth, E.; Miller, A. A.; McLaughlin, R. E.; Blinn, C. M.; Chen, A.; Nayar, A. S.; Dangel, B.; Tsai, A. S.; Rooney, M. T.; Murphy-Benenato, K. E.; Eakin, A. E.; Nicolau, D. P., Pharmacodynamic Profiling of a Siderophore-Conjugated Monocarbam in Pseudomonas aeruginosa: Assessing the Risk for

Resistance and Attenuated Efficacy. *Antimicrob. Agents Chemother.* **2015,** *59* (12), 7743-7752 DOI 10.1128/aac.00831-15.

18. Ito, A.; Nishikawa, T.; Matsumoto, S.; Yoshizawa, H.; Sato, T.; Nakamura, R.; Tsuji, M.; Yamano, Y., Siderophore Cephalosporin Cefiderocol Utilizes Ferric Iron Transporter Systems for Antibacterial Activity against Pseudomonas aeruginosa. *Antimicrob. Agents Chemother.* **2016,** *60* (12), 7396-7401 DOI 10.1128/aac.01405-16.

19. Vennerstrom, J. L.; Arbe-Barnes, S.; Brun, R.; Charman, S. A.; Chiu, F. C.; Chollet, J.; Dong, Y.; Dorn, A.; Hunziker, D.; Matile, H.; McIntosh, K.; Padmanilayam, M.; Santo Tomas, J.; Scheurer, C.; Scorneaux, B.; Tang, Y.; Urwyler, H.; Wittlin, S.; Charman, W. N., Identification of an antimalarial synthetic trioxolane drug development candidate. *Nature* **2004,** *430* (7002), 900-904 DOI 10.1038/nature02779.

20. Charman, S. A.; Arbe-Barnes, S.; Bathurst, I. C.; Brun, R.; Campbell, M.; Charman, W. N.; Chiu, F. C.; Chollet, J.; Craft, J. C.; Creek, D. J.; Dong, Y.; Matile, H.; Maurer, M.; Morizzi, J.; Nguyen, T.; Papastogiannidis, P.; Scheurer, C.; Shackleford, D. M.; Sriraghavan, K.; Stingelin, L.; Tang, Y.; Urwyler, H.; Wang, X.; White, K. L.; Wittlin, S.; Zhou, L.; Vennerstrom, J. L., Synthetic ozonide drug candidate OZ439 offers new hope for a single-dose cure of uncomplicated malaria. *Proc. Natl. Acad. Sci. U S A* **2011,** *108* (11), 4400-4405 DOI 10.1073/pnas.1015762108.

21. Mahajan, S. S.; Deu, E.; Lauterwasser, E. M.; Leyva, M. J.; Ellman, J. A.; Bogyo, M.; Renslo, A. R., A fragmenting hybrid approach for targeted delivery of multiple therapeutic agents to the malaria parasite. *ChemMedChem* **2011,** *6* (3), 415-419 DOI 10.1002/cmdc.201100002.

22. Fontaine, S. D.; Spangler, B.; Gut, J.; Lauterwasser, E. M.; Rosenthal, P. J.; Renslo, A. R., Drug delivery to the malaria parasite using an arterolane-like scaffold. *ChemMedChem* **2015,** *10* (1), 47-51 DOI 10.1002/cmdc.201402362.

23. Deu, E.; Chen, I. T.; Lauterwasser, E. M.; Valderramos, J.; Li, H.; Edgington, L. E.; Renslo, A. R.; Bogyo, M., Ferrous iron-dependent drug delivery enables controlled and selective release of therapeutic agents in vivo. *Proc. Natl. Acad. Sci. U S A* **2013,** *110* (45), 18244-18249 DOI 10.1073/pnas.1312782110.

24. Lauterwasser, E. M.; Fontaine, S. D.; Li, H.; Gut, J.; Katneni, K.; Charman, S. A.; Rosenthal, P. J.; Bogyo, M.; Renslo, A. R., Trioxolane-Mediated Delivery of Mefloquine Limits Brain Exposure in a Mouse Model of Malaria. *ACS Med. Chem. Lett.* **2015,** *6* (11), 1145-1149 DOI 10.1021/acsmedchemlett.5b00296.

25. Spangler, B.; Fontaine, S. D.; Shi, Y.; Sambucetti, L.; Mattis, A. N.; Hann, B.; Wells, J. A.; Renslo, A. R., A Novel Tumor-Activated Prodrug Strategy Targeting Ferrous Iron Is Effective in Multiple Preclinical Cancer Models. *J. Med. Chem.* **2016,** *59* (24), 11161-11170 DOI 10.1021/acs.jmedchem.6b01470.

26. Spangler, B.; Morgan, C. W.; Fontaine, S. D.; Vander Wal, M. N.; Chang, C. J.; Wells, J. A.; Renslo, A. R., A reactivity-based probe of the intracellular labile ferrous iron pool. *Nat. Chem. Biol.* **2016,** *12* (9), 680-685 DOI 10.1038/nchembio.2116.

27. Aron, A. T.; Heffern, M. C.; Lonergan, Z. R.; Vander Wal, M. N.; Blank, B. R.; Spangler, B.; Zhang, Y.; Park, H. M.; Stahl, A.; Renslo, A. R.; Skaar, E. P.; Chang, C. J., In vivo bioluminescence imaging of iron accumulation in a murine model of Acinetobacter baumannii infection. *Proc. Natl. Acad. Sci. USA* **2017,** *114* (48), 12669–12674 DOI 10.1073/pnas.1708747114.

28. Aloush, V.; Navon-Venezia, S.; Seigman-Igra, Y.; Cabili, S.; Carmeli, Y., Multidrug-resistant Pseudomonas aeruginosa: risk factors and clinical impact. *Antimicrob. Agents Chemother.* **2006,** *50* (1), 43-48 DOI 10.1128/aac.50.1.43-48.2006.

29. van Duin, D.; Kaye, K. S.; Neuner, E. A.; Bonomo, R. A., Carbapenem-resistant Enterobacteriaceae: a review of treatment and outcomes. *Diagn. Microbiol. Infect. Dis.* **2013,** *75* (2), 115-120 DOI 10.1016/j.diagmicrobio.2012.11.009.

30. Burrows, L. L., The Therapeutic Pipeline for Pseudomonas aeruginosa Infections. *ACS Infect. Dis.* **2018,** *4* (7), 1041-1047 DOI 10.1021/acsinfecdis.8b00112.

31. Whitfield, C.; Trent, M. S., Biosynthesis and export of bacterial lipopolysaccharides. *Annu. Rev. Biochem* **2014,** *83*, 99-128 DOI 10.1146/annurev-biochem-060713-035600.

32. Erwin, A. L., Antibacterial Drug Discovery Targeting the Lipopolysaccharide Biosynthetic Enzyme LpxC. *Cold Spring Harb. Perspect. Med* .**2016,** *6* (7), a025304 DOI 10.1101/cshperspect.a025304.

33. Tomaras, A. P.; McPherson, C. J.; Kuhn, M.; Carifa, A.; Mullins, L.; George, D.; Desbonnet, C.; Eidem, T. M.; Montgomery, J. I.; Brown, M. F.; Reilly, U.; Miller, A. A.; O'Donnell, J. P., LpxC inhibitors as new antibacterial agents and tools for studying regulation of lipid A biosynthesis in Gram-negative pathogens. *MBio* **2014,** *5* (5), e01551-14 DOI 10.1128/mBio.01551-14.

34. Vandenbroucke, R. E.; Libert, C., Is there new hope for therapeutic matrix metalloproteinase inhibition? *Nat. Rev. Drug Discov.* **2014,** *13* (12), 904-927 DOI 10.1038/nrd4390.

35. Shen, S.; Kozikowski, A. P., Why Hydroxamates May Not Be the Best Histone Deacetylase Inhibitors--What Some May Have Forgotten or Would Rather Forget? *ChemMedChem* **2016,** *11* (1), 15-21 DOI 10.1002/cmdc.201500486.

36. Fontaine, S. D.; DiPasquale, A. G.; Renslo, A. R., Efficient and stereocontrolled synthesis of 1,2,4-trioxolanes useful for ferrous iron-dependent drug delivery. *Org. Lett.* **2014,** *16* (21), 5776-5779 DOI 10.1021/ol5028392.

37. Montgomery, J. I.; Brown, M. F.; Reilly, U.; Price, L. M.; Abramite, J. A.; Arcari, J.; Barham, R.; Che, Y.; Chen, J. M.; Chung, S. W.; Collantes, E. M.; Desbonnet, C.; Doroski, M.; Doty, J.; Engtrakul, J. J.; Harris, T. M.; Huband, M.; Knafels, J. D.; Leach, K. L.; Liu, S.; Marfat, A.; McAllister, L.; McElroy, E.; Menard, C. A.; Mitton-Fry, M.; Mullins, L.; Noe, M. C.; O'Donnell, J.; Oliver, R.; Penzien, J.; Plummer, M.; Shanmugasundaram, V.; Thoma, C.; Tomaras, A. P.; Uccello, D. P.; Vaz, A.; Wishka, D. G., Pyridone methylsulfone hydroxamate LpxC inhibitors for the treatment of serious gram-negative infections. *J. Med. Chem.* **2012,** *55* (4), 1662-1670 DOI 10.1021/jm2014875.

38. *Methods for Dilution Antimicrobial Susceptibility Tests for Bacteria That Grow Aerobically; Approved Standard—Ninth Edition.* CLSI, 950 West Valley Road, Suite 2500, Wayne, Pennsylvania 19087 USA, 2015.

39. *Performance Standards for Antimicrobial Susceptibility Testing; Twenty-Seventh Informational Supplement.* CLSI, 940 West Valley Road, Suite 1400, Wayne, Pennsylvania 19087-1898 USA, 2016.

40. Tyrrell, J.; Callaghan, M., Iron acquisition in the cystic fibrosis lung and potential for novel therapeutic strategies. *Microbiology* **2016,** *162* (2), 191-205 DOI 10.1099/mic.0.000220.

41. Hunter, R. C.; Asfour, F.; Dingemans, J.; Osuna, B. L.; Samad, T.; Malfroot, A.; Cornelis, P.; Newman, D. K., Ferrous iron is a significant component of bioavailable iron in cystic fibrosis airways. *MBio* **2013,** *4*, e00557-13 DOI 10.1128/mBio.00557-13.

42. Wakeman, C. A.; Moore, J. L.; Noto, M. J.; Zhang, Y.; Singleton, M. D.; Prentice, B. M.; Gilston, B. A.; Doster, R. S.; Gaddy, J. A.; Chazin, W. J.; Caprioli, R. M.; Skaar, E. P., The innate immune protein calprotectin promotes Pseudomonas aeruginosa and Staphylococcus aureus interaction. *Nat. Commun.* **2016,** *7*, 11951 DOI 10.1038/ncomms11951.

TOC Graphic

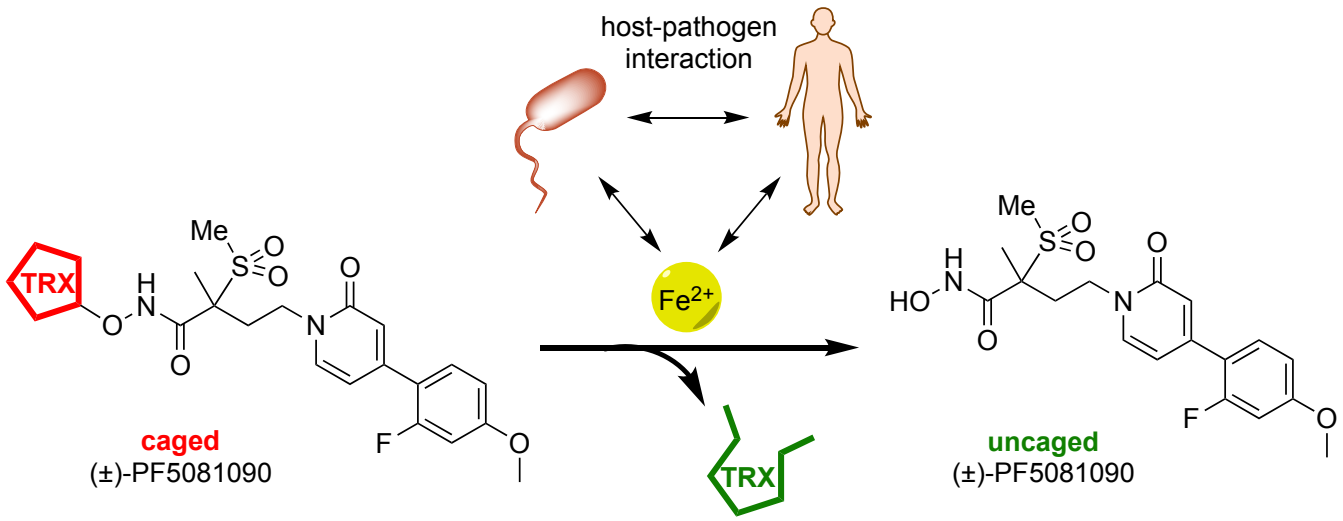
host-pathogen
interaction
TRX
Me
S
O
O
H
N
O
O
N
O
F
O
caged
(±)-PF5081090
Fe2+
TRX
Me
S
O
O
HO
H
N
O
N
O
F
O
uncaged
(±)-PF5081090